Research paper

Numerical estimation of blast wave strength from an underground structure

Yuta Sugiyama*†, Kunihiko Wakabayashi*, Tomoharu Matsumura*, and Yoshio Nakayama*

*National Institute of Advanced Industrial Science and Technology (AIST),
Central 5, 1−1−1 Higashi, Tsukuba, Ibaraki 305−8565, JAPAN
Phone : +81−29−861−0552
†Corresponding author : yuta.sugiyama@aist.go.jp

Received : August 22, 2014 Accepted : October 10, 2014

Abstract

This paper shows the propagation phenomenon of a blast wave from an explosion originating inside an underground structure. We numerically and theoretically estimate the blast wave strength from the simplest two-dimensional axisymmetric underground structure in order to discuss mitigation effects on a blast wave on the ground from the structural advantage. Height H and diameter D of the underground structure are the parameters used in this study. A small height H does not show any mitigation effect on a blast wave on the ground at a distance far from the underground structure. When H is larger than critical height H^*, depending on D, the peak overpressures on the ground are mitigated, and the increment of H has a far greater mitigation effect. The shock pressure inside the underground structure is estimated by the one-dimensional shock tube problem, which determines critical height H^* and shock pressure distribution p_s with respect to height. Shock pressure $p_s(H)$ in an underground structure exit can scale the strength of the blast wave on the ground.

Keywords : numerical simulation, subsurface magazine, mitigation, blast wave

1. Introduction

High explosives are used widely in industrial operations such as mining and blasting excavation because of the instantaneous release of their powerful energy. However, an unexpected explosion generates a blast wave, the peak overpressure of which causes damage having a severity dependent on the distance between the magazine where the explosive is stored and adjacent residential areas. Therefore, it is necessary to develop a magazine that reduces peak overpressure as efficiently as possible. Subsurface magazines, which are constructed underground, have been proposed as a suitable type of magazine[1)−5)]. A subsurface magazine has a vertical elevator that serves as the exit path from the storage chamber. When an explosion occurs, a blast wave and a high-speed jet are generated, which exit the subsurface magazine via this opening. As a high-speed jet propagating normal to the ground has little effect on the propagation of a blast wave on the ground, the structural advantage of a subsurface magazines results in a mitigation of the blast wave and a reduction of fragments on the ground. Saburi et al.[1),2)] described experimental studies on debris hazards and ground vibration resulting from explosions in subsurface magazines. Nakayama et al.[3)] conducted experiments with a subsurface magazine, and their results showed obvious blast wave mitigation, as compared with the case of a surface explosion. However, the basic data needed to discuss the mitigation effect of a subsurface magazine, such as the relation between blast wave strength and the configuration of the subsurface magazine, are lacking. Therefore, in this paper, as a first step, we numerically estimate the blast wave strength from the simplest two-dimensional axisymmetric underground structure in order to discuss its structural advantage and mitigation effect theoretically.

2. Numerical methods

The governing equations are two-dimensional axisymmetric compressible Euler equations in generalized coordinates. The fluid is modeled as an ideal gas with a constant specific heat ratio, $\gamma = 1.4$, and all diffusive effects are neglected. These equations are discretized using the

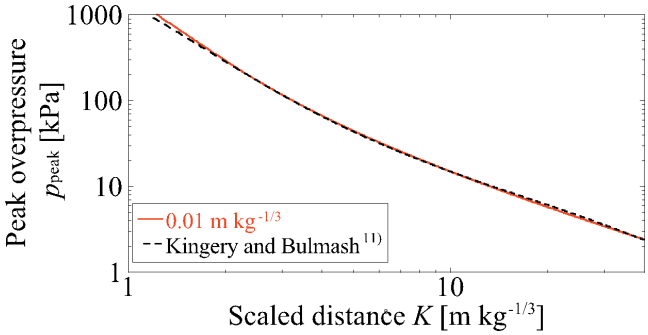

Figure 1 Peak overpressure distribution of a hemispherical explosion for a grid spacing of 0.01 m kg$^{-1/3}$, along with the empirical formula of Kingery and Bulmash. The horizontal axis indicates the scaled distance K m kg$^{-1/3}$.

third-order Harten-Lax-van Leer (HLL)-Harten-Lax-van Leer for contact (HLLC) scheme by monotonic upstream-centered scheme for conservation laws (MUSCL) interpolation with a linear scaling limiter[6)–9)]. The switching of the HLL and HLLC schemes is determined by the pressure differences between a grid point and the other points around it. The three-stage TVD Runge-Kutta method is used for time integration. Our data, as well as those from our previous paper[10)], incorporate a scaled distance, m kg$^{-1/3}$ by the mass of the explosive.

First, we conduct a hemispherical explosion to verify our numerical methods and conduct a grid convergence study by comparison with the empirical curve of Kingery and Bulmash[11)]. In this study, the hemispherical high-pressure gas has the same energy as 1 kg of TNT (4.29 MJ kg^{-1}). In the radial direction, the grid size of 0.01 m kg$^{-1/3}$ is distributed uniformly in the calculation domain. Figure 1 shows the peak overpressure distribution of the hemispherical explosion in this study, along with the empirical formula of Kingery and Bulmash[11)]. In Figure 1, the results of the calculations used in this paper show good agreement with the empirical curve in the grid spacing. We calculate the explosion in the underground structure under the condition that the grid spacing is 0.01 m kg$^{-1/3}$ in all regions.

Figure 2 shows a schematic diagram of the calculation target with boundary conditions and the initial condition of the high explosive. Here, l and d respectively denote the length and the diameter of the high explosive. As shown in Figure 2, an explosion occurs by a basement wall along the central axis of the chamber, and a high explosive of TNT (4.29 MJ kg^{-1}) is modeled as cylindrical high-energy atmosphere. The mass is constant at $m = 1$ kg, and the length of the high explosive is $l = 0.1$ m kg$^{-1/3}$. Its shape is cylindrical and the ratio of length to diameter l/d is 1. H and D, respectively, indicate the height and the diameter of the underground structure and are the parameters used in this study. The point of origin is the center of the underground structure exit on the ground. The colored boundary conditions are described below. For the axisymmetric calculations, the axis boundary condition is shown by a blue dashed line. The slip wall and the extrapolation conditions for other boundaries are shown by green and orange lines, respectively.

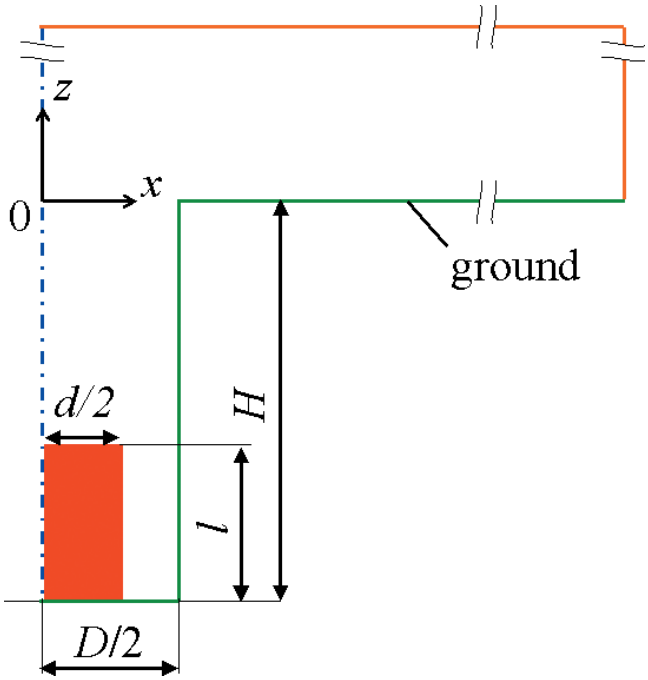

Figure 2 Schematic diagram of the calculation target with boundary conditions and initial condition of high explosive denoted as red zone. l, d, D and H respectively denote the length and the diameter of the high explosive, and the height and the diameter of the underground structure. The point of origin is the center of the underground structure exit on the ground. Blue dashed line shows the axis boundary condition. Green and orange lines show the slip wall and the extrapolation conditions for other boundaries.

3. Results and Discussions

3.1 Flow patterns and blast wave strength

Figure 3 shows snapshots of the absolute gradient of density at $0 \le x$ m kg$^{-1/3} \le 3.8$ and $-0.2 \le z$ m kg$^{-1/3} \le 5.2$ in the case of $D = 0.2$ m kg$^{-1/3}$ and $H = 2$ m kg$^{-1/3}$. Inside the underground structure, a shock wave is generated and propagates vertically to the exit. After the arrival of the shock wave at the exit, the blast wave expands elliptically into the open space at 1.78 ms in Figure 3a due to the hypersonic jet that propagates vertical to the ground behind the shock wave. Near the exit, complicated shock patterns appear including Mach disk, barrel shock, and reflected shock, as is often observed in a hypersonic jet from a nozzle. At 4.43 ms in Figure 3b, a vortex is induced by fluid dynamic instabilities such as Richtmyer-Meshkov instability, and its local acceleration generates shock waves propagating to the blast wave. The shock waves will collide with and strengthen the blast wave. A long-duration jet induced by the shock wave continues to flow vertically to the ground. The inset view of Figure 3c at 6.65 ms shows the shock cell structure that strengthens fluid dynamic instability.

For safety analysis, we focus on peak overpressures and propagation of the blast wave on the ground. Figure 4 shows the peak overpressure distributions on the ground surface ($z = 0$) in the cases of an underground explosion

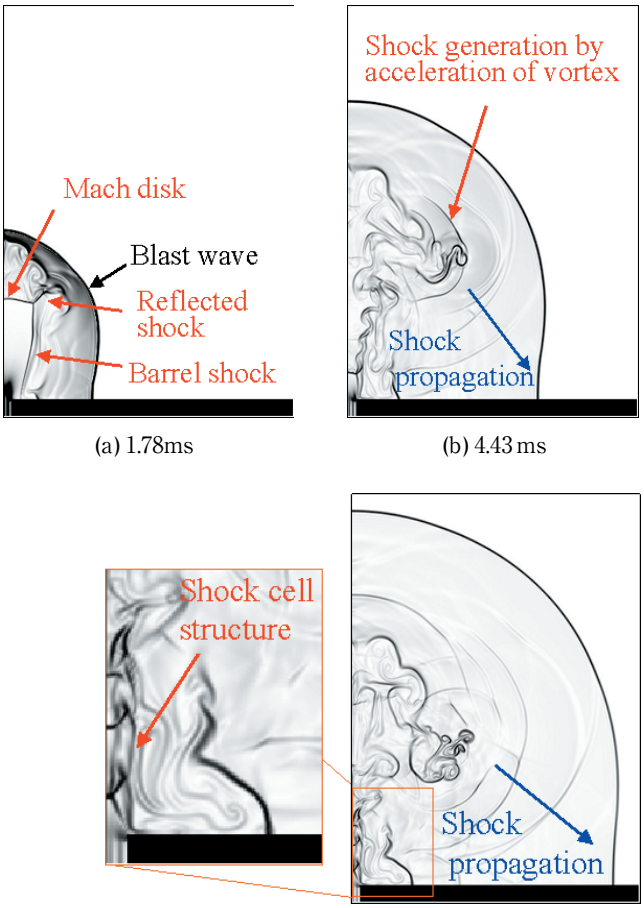

(a) 1.78ms (b) 4.43 ms

(c) 6.65 ms

Figure 3 Instantaneous pictures of absolute gradient of density at $0 \leq x$ m kg$^{-1/3}$ ≤ 3.8 and $-0.2 \leq z$ m kg$^{-1/3} \leq 5.2$.

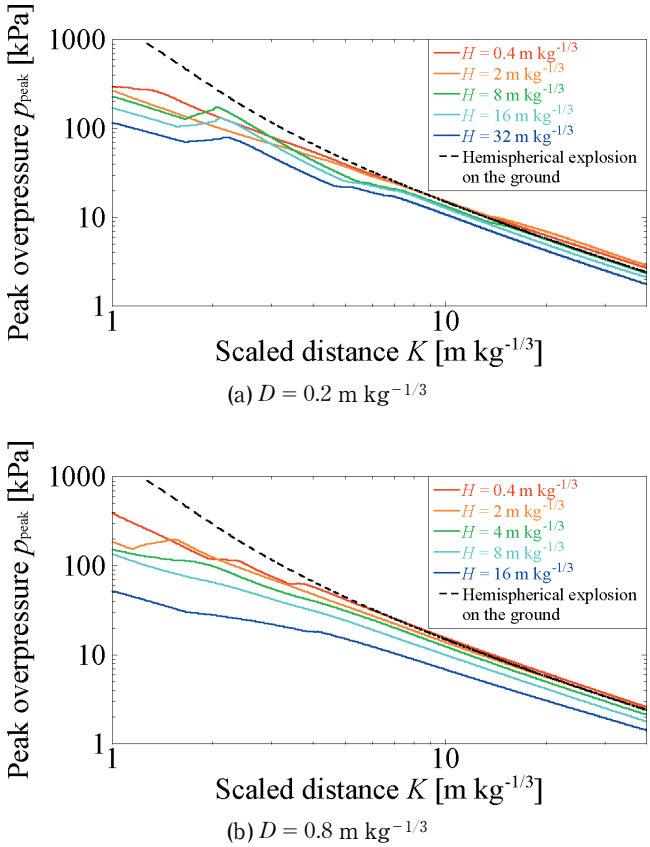

(a) $D = 0.2$ m kg$^{-1/3}$

(b) $D = 0.8$ m kg$^{-1/3}$

Figure 4 Peak overpressure distributions on the ground surface ($z = 0$) for an underground explosion and a hemispherical explosion. The horizontal axis denotes the scaled distance K m kg$^{-1/3}$ in x direction.

and a hemispherical explosion. In Figures 4a and 4b, the diameters of the underground structure are $D = 0.2$ mkg$^{-1/3}$ and 0.8 m kg$^{-1/3}$, respectively. The horizontal axis indicates the scaled distance K in x direction. In all cases, the structural advantage has a mitigation effect on the blast wave at smaller K. Shock waves, which are generated by the movement of the vortex in Figure 3, reach the blast wave, and its strength recovers at several points. When $H = 0.4$ m kg$^{-1/3}$ and 2 m kg$^{-1/3}$ in Figure 4a and $H = 0.4$ m kg$^{-1/3}$ in Figure 4b, the peak overpressures p_{peak} at larger K agrees well with that of the hemispherical explosion. This indicates that the small height H does not show a mitigation effect at a distance far from the underground structure. When H becomes larger than the critical value, the peak overpressures p_{peak} becomes small, and the increment of H has a much greater mitigation effect on the blast wave. At the same height of 8 and 16 m kg$^{-1/3}$, the mitigation effect becomes strong in the case of larger diameter D.

3.2 Simple estimation method for blast wave strength at the exit of an underground structure

Previous studies[12),13)] give the empirical formulations of exit and exterior pressure distributions outside ammunition storage facilities. They show that the exit pressure determines the blast wave strength in an open space. Here, we discuss and estimate the shock wave strength at the exit of an underground structure. Figure 5 shows the calculation targets in this section. Figure 5a (Case 1) denotes the same condition of $H \sim \infty$ as in Figure 2, whereas Figure 5b (Case 2) denotes that the high explosive attaches to a sidewall of the underground structure in order to assume the one-dimensional shock tube problem. The origin of the ζ axis is located at the interface between the atmosphere and the high explosive. The colored boundaries represent the same conditions as described in Section 2. The shock tube problem shows that a generated shock wave maintains until the expansion wave from the basement wall meets the shock wave in Figure 5. In order to describe a similar trajectory of the expansion wave in the ζ direction, the length of the high explosive, l, should be the same, and therefore, it is constant in the estimation between Cases 1 and 2. As the energy of the high explosive is constant at 1 kg of TNT (4.2 MJ kg^{-1}), the density and pressure in Case 2 are smaller than those in Case 1.

Figure 6 shows the shock pressure distributions at the tube axis, and the horizontal axis denotes the height of the underground structure ζ. Red and blue lines denotes the shock pressure distributions in the Case 1 and 2, respectively. Shock tube theory gives that the shock wave maintains its strength before the expansion wave affects the shock wave. Points in (a) and (b) denote the constant shock pressure p_s^* and its end point ζ^* estimated by Case 2. Here, ζ^* is defined as the point at which shock pressure

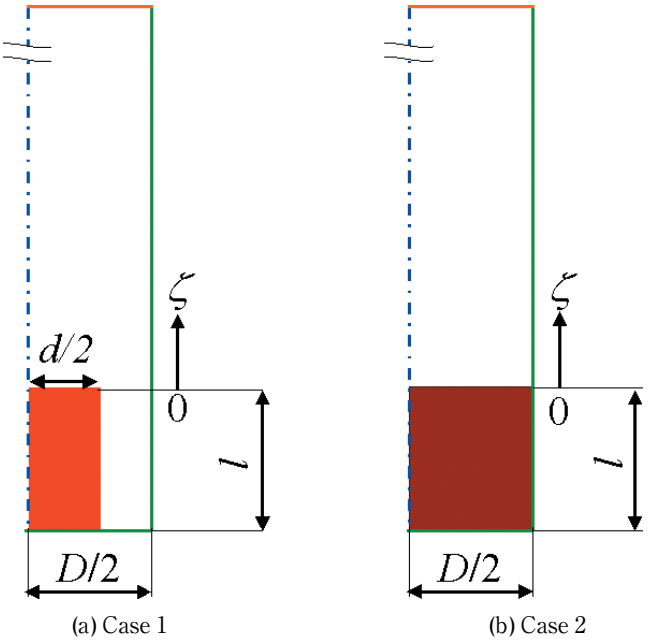

(a) Case 1 (b) Case 2

Figure 5 Calculation targets. Case 1 denotes the same condition of $H \sim \infty$ as in Figure 2, whereas Case 2 denotes that a high explosive is attached to a sidewall of the underground structure. Red colored zones denote the high explosive. l, d, and D respectively denote the length and the diameter of the high explosive, and the diameter of the underground structure. The origin of the ζ axis is located at the interface between the atmosphere and the high explosive. Blue dashed line shows the axis boundary condition. Green and orange lines show the slip wall and the extrapolation conditions for other boundaries.

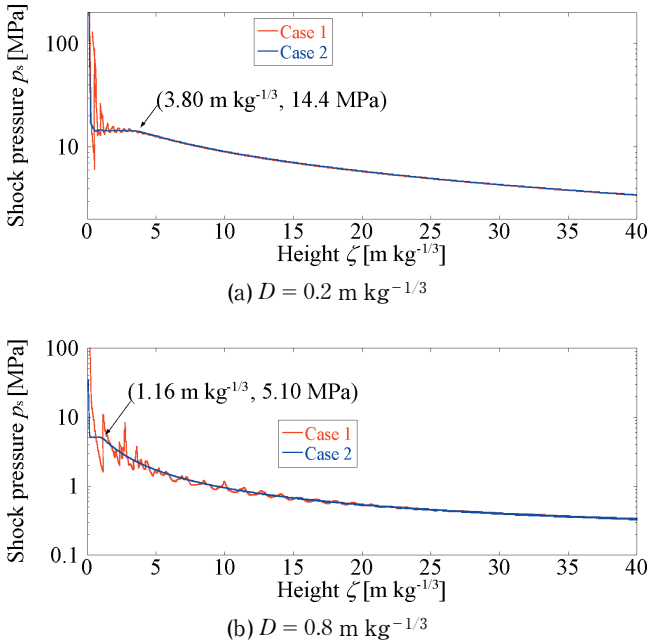

Figure 6 Shock pressure distributions at the tube axis ($x = 0$). The horizontal axis denotes ζ in Figure 5. Points in (a) and (b) denote the constant shock pressure p_s^* and its end point ζ^* by Case 2. Red and blue lines denote the shock pressure distributions in the Case 1 and 2, respectively.

$p_s = 0.995\ p_s^*$. When $\zeta > \zeta^*$, the expansion wave weakens the shock wave, and its pressure decreases. At $D = 0.2$ m kg$^{-1/3}$ and 0.8 m kg$^{-1/3}$, ζ^* and p_s^* are 3.80 m kg$^{-1/3}$ and 14.4 MPa, and 1.16 m kg$^{-1/3}$ and 5.10 MPa, respectively. In Figure 5a, as the high explosive does not attach to the sidewall in Case 1, transverse waves successively reflect off the tube axis, and shock pressure oscillation occurs. This indicates that it is difficult to estimate the shock pressure, especially for a small ζ. In Case 2, a one-dimensional shock wave is generated, and no oscillation occurs. The shock pressure distribution in Case 1 agrees with that in Case 2, which indicates that the shock pressure $p_s(\zeta)$ can be estimated by the one-dimensional shock tube problem with diluent high-pressure gas as shown in Figure 5b. Shock pressure distribution in Case 2 shows the characteristics that the shock pressure becomes a constant value p_s^* at $\zeta < \zeta^*$, and gradually decreases at $\zeta > \zeta^*$ by the expansion wave from the basement wall. Figures 2 and 5 show that the height of the underground structure is calculated as $H = \zeta + l$. As the exit pressure determines the blast wave strength, it is assumed that the shock pressure $p_s(H)$ can approximate that at the exit of the underground structure in Figure 2 and that no mitigation effect of the blast wave on the ground appears at a distance far from the underground structure when $H < \zeta^* + l$.

In order to estimate the strength of the shock wave, we theoretically calculate the important values from the shock tube problem as shown in the schematic of the propagation of waves in Figure 7. P_1 denotes the point where the expansion front wave F reflects off the basement wall ($\zeta = -l_4$). P_2, P_3, and P_4 indicate the points where the reflected expansion front wave F catches up with the expansion back wave B, the contact surface C and the shock wave S, respectively. Here, critical height H^* is defined as the distance between the wall and the point that the expansion wave F meets the shock wave S. As shown in Figure 6, the shock pressure remains constant until the reflected expansion wave F meets the shock wave S at ζ_4 in Figure 7. Now, ζ_4 is calculated theoretically by simple shock tube theory[14]. We assume that all fluids are modeled by the ideal gas equation of state. γ_1 and γ_4 respectively denote the specific heat ratios of the driven and driver gas and are constant at $\gamma_1 = \gamma_4 = \gamma = 1.4$. In the initial condition, the pressure and speed of sound of driven gas are $p_1 = 101325$ Pa and $a_1 = 343.8$ ms^{-1}. Pressure p_4 and speed of sound a_4 of driver gas are calculated by

$$p_4 = (\gamma_4 - 1)\rho_4\varepsilon_4 = (\gamma_4 - 1)\frac{4m}{\pi D^2 l_4}\varepsilon_4, \tag{1}$$

and

$$a_4 = \sqrt{\frac{\gamma_4 p_4}{\rho_4}} = \sqrt{\gamma_4(\gamma_4 - 1)\varepsilon_4}, \tag{2}$$

where, m, ρ_4, ε_4, and l_4 are the mass of the high explosive, density, internal energy per unit mass, and the length of the driver gas region. The speed of sound a_4 does not depend on the size of l_4 and D. Mach number M_s and shock pressure p_2^* of shock wave S are obtained by solving

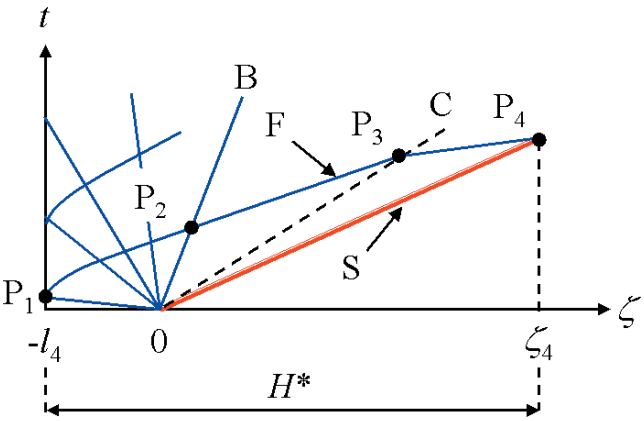

Figure 7 Schematic diagram of the propagation of waves in the shock tube problem in the $\zeta - t$ plane. P_1 denotes the point where expansion front wave F reflects off the basement wall. P_2, P_3, and P_4 indicate the points where the reflected expansion front wave F catches up with the expansion back wave B, the contact surface C and the shock wave S, respectively. H^* denotes the critical height between the wall and the point that the expansion wave F meets the shock wave S.

$$\frac{p_4}{p_1} = \frac{2\gamma_1 M_s^2 - (\gamma_1 - 1)}{\gamma_1 + 1}\left[1 - \frac{\gamma_4 - 1}{\gamma_1 + 1}\frac{a_1}{a_4}\left(M_s - \frac{1}{M_s}\right)\right]^{-\frac{2\gamma_4}{\gamma_4 - 1}} \tag{3}$$

and

$$\frac{p_2^*}{p_1} = \frac{2\gamma_1 M_s^2 - (\gamma_1 - 1)}{\gamma_1 + 1}. \tag{4}$$

Velocity u_2 and the speed of sound a_2 of the hot gas behind the shock wave S are calculated using

$$\frac{u_2}{a_1} = \frac{2}{\gamma_1 + 1}\left(M_s - \frac{1}{M_s}\right) \tag{5}$$

and

$$\left(\frac{a_2}{a_1}\right)^2 = \frac{[2\gamma_1 M_s^2 - (\gamma_1 - 1)][(\gamma_1 - 1)M_s^2 + 2]}{(\gamma_1 + 1)^2 M_s^2} \tag{6}$$

Using these values in Equations (1) through (6), the times t and positions ζ of P_1, P_2, P_3, and P_4 are described as follows:

$$\zeta_1 = -l_4, \tag{7}$$

$$t_1 = \frac{l_4}{a_4}, \tag{8}$$

$$\zeta_2 = l_4\left\{2\left[\frac{\gamma_4 - 1}{\gamma_1 + 1}\frac{a_1}{a_4}\left(M_s - \frac{1}{M_s}\right)\right] - 1\right\} \left[1 - \frac{\gamma_4 - 1}{\gamma_1 + 1}\frac{a_1}{a_4}\left(M_s - \frac{1}{M_s}\right)\right]^{-\frac{\gamma_4 + 1}{2(\gamma_4 - 1)}}, \tag{9}$$

$$t_2 = t_1\left[1 - \frac{\gamma_4 - 1}{\gamma_1 + 1}\frac{a_1}{a_4}\left(M_s - \frac{1}{M_s}\right)\right]^{-\frac{\gamma_4 + 1}{2(\gamma_4 - 1)}} \tag{10}$$

$$\zeta_3 = l_4\frac{4}{\gamma_1 + 1}\frac{a_1}{a_4}\left(M_s - \frac{1}{M_s}\right)\left[1 - \frac{\gamma_4 - 1}{\gamma_1 + 1}\frac{a_1}{a_4}\left(M_s - \frac{1}{M_s}\right)\right]^{-\frac{\gamma_4 + 1}{2(\gamma_4 - 1)}} \tag{11}$$

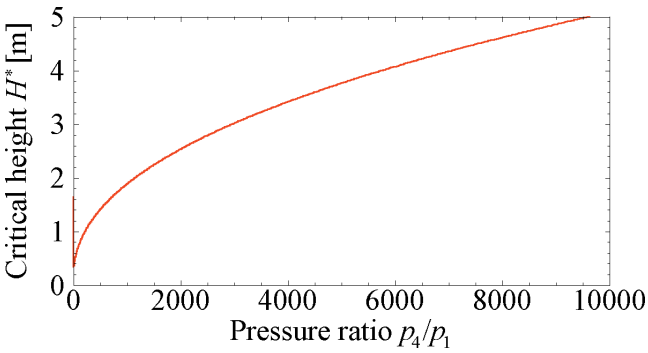

Figure 8 Relation between critical height H^* and pressure ratio p_4/p_1 at $l_4 = l = 0.1$ m kg$^{-1/3}$, $\varepsilon_4 = 4.29$ MJ kg^{-1}, and $m = 1$ kg.

$$t_3 = 2t_1\left[1 - \frac{\gamma_4 - 1}{\gamma_1 + 1}\frac{a_1}{a_4}\left(M_s - \frac{1}{M_s}\right)\right]^{-\frac{\gamma_4 + 1}{2(\gamma_4 - 1)}} \tag{12}$$

$$\zeta_4 = H^* - l_4 = M_1 a_1 \frac{\zeta_3 - (u_2 + a_2)t_3}{M_1 a_1 - (u_2 + a_2)}, \tag{13}$$

and

$$t_4 = \frac{\zeta_3 - (u_2 + a_2)t_3}{M_1 a_1 - (u_2 + a_2)}. \tag{14}$$

When we apply the above idea to the explosion inside the underground structure in this study, critical height H^* in Figure 6 is equivalent of $\zeta_4 + l_4$ in Figure 7. Figure 8 shows the relation between H^* and initial pressure ratio p_4/p_1 at $l_4 = l = 0.1$ m kg$^{-1/3}$, $\varepsilon_4 = 4.29$ MJ kg^{-1}, and $m = 1$ kg calculated by the equations above. p_4/p_1, H^*, and p_2^* are calculated as 5390, 3.89 m kg$^{-1/3}$, and 14.4 MPa for $D = 0.2$ m kg$^{-1/3}$, and 337, 1.19 m kg$^{-1/3}$, and 5.10 MPa for $D = 0.8$ m kg$^{-1/3}$, which agree well with data in Figure 6. Therefore, the one-dimensional shock tube problem determines the critical height H^* and shock pressure p_2^*. Shock pressure at arbitrary H, $p_s(H)$ can be estimated by Figure 6.

3.3 Rescaling method for blast wave strength on the ground

The previous section shows that shock pressure p_s at height $H = \zeta + l_4$ is estimated by solving the one-dimensional shock tube problem. Using the shock pressure at exit $p_s(H)$ in Figure 6, peak overpressure p_{peak} is scaled by

$$p_{peak}^* = p_{peak}\left(\frac{p_s(H)}{p_2^*}\right)^n = p_{peak}\theta^n. \tag{15}$$

Here, θ indicates the pressure ratio of $p_s(H)/p_2^*$ calculated from Case 2 in Figure 6. n is an arbitrary number and 1/3 in this study. Figure 9 shows the peak overpressure distributions on the ground surface ($z = 0$) in the cases of underground explosion at (a) $D = 0.2$ m kg$^{-1/3}$ and (b) $D = 0.8$ m kg$^{-1/3}$ where $n = 1/3$ in Equation (15). The horizontal and vertical axes denote the scaled distance K in x direction and scaled peak overpressure p_{peak}^*. At the simulated height H in this study, the peak overpressures p_{peak}^* at large scaled distance K shows a

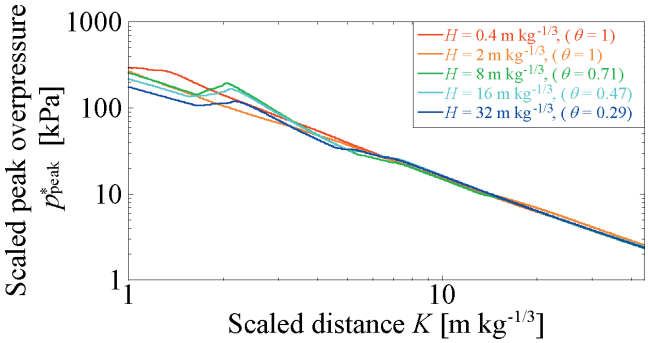

(a) $D = 0.2$ m kg$^{-1/3}$

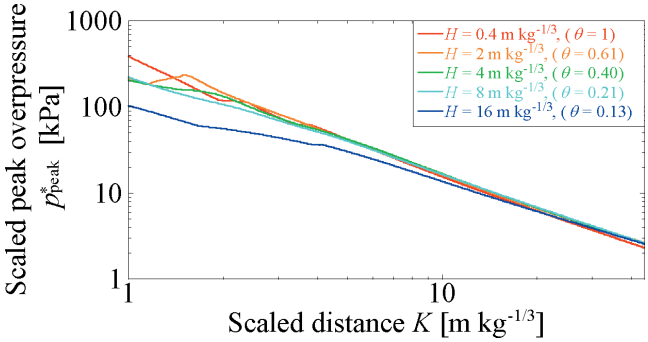

(b) $D = 0.8$ m kg$^{-1/3}$

Figure 9 Peak overpressure distributions on the ground surface ($z = 0$) for an underground explosion where $n = 1/3$ in Equation (15). The horizontal and vertical axes denote the scaled distance K in x direction and scaled peak overpressure p^*_{peak}.

unique profile. This indicates that the exit pressure from the underground structure determines the strength of the blast wave and the proper arbitrary number ($n = 1/3$ in this study for 0.4 m kg$^{-1/3} \le H \le 32$ m kg$^{-1/3}$ and 0.2 m kg$^{-1/3} \le D \le 0.8$ m kg$^{-1/3}$).

As our study considers an explosion inside the simplest two-dimensional axisymmetric underground structure, it is difficult to directly use Equations 1–14 for the arbitrary configuration of an underground structure. However, when a proper method to estimate the propagation of waves such as a shock wave and an expansion wave inside an underground structure is utilized, the blast wave strength on the ground can be estimated.

4. Conclusion

We performed numerical calculations for the simplest axisymmetric two-dimensional underground structure to investigate the blast wave strength on the ground. Flow patterns showed that the shock wave inside the underground structure expanded as an elliptical blast wave from the exit. The hypersonic flow induced by the shock wave created a vortex, long-duration jet vertically to the ground and complicated shock patterns. We discussed and estimated the blast wave strength on the ground. The one-dimensional shock tube problem can be used to estimate the critical height that maintains constant shock pressure inside an underground structure, and the shock pressure depending on the height of the underground structure. The exit pressure from the underground structure can scale the strength of the blast wave on the ground.

References

1) T. Saburi, S. Kubota, K. Katoh, and Y. Ogata, Sci. Tech. Energetic Materials, 74, 53–60 (2013).
2) T. Saburi, S. Kubota, K. Katoh, and Y. Ogata, Sci. Tech. Energetic Materials, 74, 85–92 (2013).
3) Y. Nakayama, K. Wakabayashi, T. Matsumura, and M. Iida, Applied Mechanics and Materials 82, 663–668 (2011).
4) K. Hasue, K. Munemasa, T. Adachi, K. Katoh, and S. Nakahara, Sci. Tech. Energetic Materials, 51, 15–21 (1990).
5) K. Hasue, K. Munemasa, T. Adachi, K. Katoh, and S. Nakahara, Sci. Tech. Energetic Materials, 51, 8–15 (1990).
6) A. Harten, P. D. Lax, and B. van Leer, SIAM Rev. 25, 35–61 (1983).
7) E. F. Toro, M. Spruce, and W. Speares, Shock Waves, 4, 25–34 (1994).
8) S. D. Kim, B. J. Lee, H. J. Lee, I. S. Jeung and J. Y. Choi, Int. J. Numer. Meth. Fluids, 62, 1107–1133 (2010).
9) X. Zhang, and C. W. Shu, Proc. Royal Society A, 467, 2752–2776 (2011).
10) Y. Sugiyama, T. Homae, K. Wakabayashi, T. Matsumura and Y. Nakayama, Sci. Tech. Energetic Materials, 75, 112–118 (2014).
11) C. N. Kingery and G. Bulmash, ARBRL–TR–02555, Ballistics Research Laboratory (1984).
12) C. N. Kingery, BRL–TR–3012, Ballistics Research Laboratory (1989).
13) C. N. Kingery, and E. J. Gion, BRL–TR–3132, Ballistics Research Laboratory (1990).
14) J. D. Anderson, "Modern Compressible Flow With Historical Perspective", 3rd Ed., (2004), McGraw-Hill.